

Acceleration of α -Synuclein Aggregation by Exosomes^{*[S]}

Received for publication, May 30, 2014, and in revised form, November 17, 2014. Published, JBC Papers in Press, November 25, 2014, DOI 10.1074/jbc.M114.585703

Marie Grey^{†1}, Christopher J. Dunning^{§¶1}, Ricardo Gaspar^{†¶1}, Carl Grey^{||}, Patrik Brundin^{§**2}, Emma Sparr^{†3}, and Sara Linse^{†4}

From the Departments of [†]Physical Chemistry, [¶]Biochemistry and Structural Biology, and ^{||}Biotechnology, the [§]Neuronal Survival Unit, Department of Experimental Medical Science, Wallenberg Neuroscience Center, Lund University, SE-22100 Lund, Sweden and the Center for Neurodegenerative Science, ^{**}The Van Andel Research Institute, Grand Rapids, Michigan 49503

Background: Cell-to-cell transmission of α -syn via exosomes has been proposed to propagate Parkinson disease pathology.

Results: Exosomes contain gangliosides, several other lipid classes, and proteins. Exosomes and ganglioside vesicles accelerate α -syn aggregation. Vesicles made of other membrane lipids do not.

Conclusion: Exosomes provide catalytic environments for nucleation of α -syn aggregation.

Significance: Revealing factors that promote α -syn aggregation may provide insight into Parkinson disease pathogenesis.

Exosomes are small vesicles released from cells into extracellular space. We have isolated exosomes from neuroblastoma cells and investigated their influence on the aggregation of α -synuclein, a protein associated with Parkinson disease pathology. Using cryo-transmission electron microscopy of exosomes, we found spherical unilamellar vesicles with a significant protein content, and Western blot analysis revealed that they contain, as expected, the proteins Flotillin-1 and Alix. Using thioflavin T fluorescence to monitor aggregation kinetics, we found that exosomes catalyze the process in a similar manner as a low concentration of preformed α -synuclein fibrils. The exosomes reduce the lag time indicating that they provide catalytic environments for nucleation. The catalytic effects of exosomes derived from naive cells and cells that overexpress α -synuclein do not differ. Vesicles prepared from extracted exosome lipids accelerate aggregation, suggesting that the lipids in exosomes are sufficient for the catalytic effect to arise. Using mass spectrometry, we found several phospholipid classes in the exosomes, including phosphatidylcholine, phosphatidylserine, phosphatidylethanolamine, phosphatidylinositol, and the gangliosides GM2 and GM3. Within each class, several species with different acyl chains were identified. We then prepared vesicles from corresponding pure lipids or defined mixtures, most of which were found to retard α -synuclein aggregation. As a striking exception, vesicles containing ganglioside lipids GM1 or GM3 accelerate the process. Understanding how α -synuclein

interacts with biological membranes to promote neurological disease might lead to the identification of novel therapeutic targets.

Extracellular vesicles are released by cells into the extracellular space. In recent years, research into these vesicles has expanded considerably with a major focus on exosomes, defined by their size and the presence of proteins such as Alix and Flotillin-1. These small vesicles of ~100 nm in diameter are used for intercellular communication. Exosomes are found in most body fluids and contain lipid, protein, and RNA. *In vitro* experiments suggest that exosomal release by neurons depends on synaptic activity and that released exosomes are taken up by other neurons (1).

Several proteins mediate vesicle secretion and trafficking in cells (2). One of these proteins, α -synuclein (α -syn)⁵, appears to play a role in regulating the recycling of synaptic vesicles (3), although its function *in vivo* is poorly understood. The 140-amino acid-long α -syn is expressed at high levels in the brain and accounts for about 1% of the total protein content in the neuronal cytosol (4). α -syn is implicated in Parkinson disease (PD), which is the second most common neurodegenerative disease and leads to an array of motor and non-motor symptoms (5, 6). One neuropathological hallmark of PD is Lewy bodies in which the main component is aggregated α -syn, but other proteins and lipids are also present (7, 8). α -syn is an aggregation-prone protein, and the formation of ordered α -syn aggregates (fibrils) is considered part of the neurodegenerative process in PD and related disorders. The nature of the toxic species is debated; both the smaller aggregates formed during the aggregation process or the process *per se* have been suggested to be toxic (9–13). In solution, α -syn is a largely unstructured

* This work was supported by the Swedish Research Council and its Linneaus Centers for Organizing Molecular Matter (to E. S. and S. L.) and Bagadilico (to M. G., C. J. D., and P. B.), the European Research Council Advanced Awards (to S. L. and P. B.), Parkinsonfonden (to C. J. D.), the Crafoord Foundation (to C. J. D.), Swedish Research Council (to S. L., E. S., and P. B.), Hjärnfonden (to P. B.), the Swedish Foundation for Strategic Research (E. S.), and by the Strong Research Environment Multipark (Multidisciplinary Research in Parkinson Disease at Lund University).

⌘ Author's Choice—Final version full access.

[S] This article contains supplemental Table S1.

¹ Both authors contributed equally to this work.

² To whom correspondence may be addressed. E-mail: patrik.brundin@vai.org.

³ To whom correspondence may be addressed. E-mail: emma.sparr@fkem1.lu.se.

⁴ To whom correspondence may be addressed. E-mail: sara.linse@biochemistry.lu.se.

⁵ The abbreviations used are: α -syn, α -synuclein; β -syn, β -synuclein; PC, phosphatidylcholine; PS, phosphatidylserine; PI, phosphatidylinositol; PE, phosphatidylethanolamine; CL, cardiolipin; DOPS, 1,2-dioleoyl-*sn*-glycero-3-phospho-L-serine sodium salt; DOPC, 1,2-dioleoyl-*sn*-glycero-3-phosphocholine; SUV, small unilamellar vesicle; PD, Parkinson disease; cryo-TEM, cryogenic transmission electron microscopy; DLS, dynamic light scattering; NTA, nanoparticle tracking analysis; AD, Alzheimer disease; amyloid β , amyloid β ; ThT, thioflavin T; Hex, hexose.

Exosomes Catalyze α -Synuclein Aggregation

protein (14, 15). Membrane-associated α -syn is partly α -helical (15, 16), whereas β -sheet-rich structures form during the aggregation process and are found in Lewy bodies, for example (17, 18).

Compelling genetic evidence supports that α -syn plays a crucial role in PD pathogenesis. Point mutations in the α -syn gene cause autosomal dominant PD; α -syn gene multiplications are associated with a parkinsonian syndrome, and single nucleotide polymorphisms in the α -syn gene are associated with increased risk for PD (19–23).

Emerging evidence suggests that aggregated α -syn spreads from cell-to-cell in a prion-like manner, resulting in transmission of aggregation and neurodegeneration (24, 25). Secreted and lipid-associated α -syn is resistant to proteolysis by the KLK6 peptidase, found in the central nervous system and cerebrospinal fluid, and is co-localized with α -syn in Lewy bodies (26). Secretion of α -syn via exosomes has been proposed to amplify and propagate PD pathology (27–31), and several studies have identified α -syn associated with exosomes (27, 32, 33). Cellular dysfunction is also proposed to increase the transfer of α -syn via exosomes (33, 34). However, the details regarding the interactions between α -syn and exosomes are not understood, and whether exosomes play an important role in PD pathogenesis is still unclear.

In this study, we use a continuous thioflavin T fluorescence assay to investigate the influence of exosomes on α -syn amyloid formation. We find that exosomes accelerate the conversion of monomeric protein to fibrillar aggregates and seek a molecular explanation for this catalysis. In an attempt to explain the acceleration of the process, we determine the molecular composition of isolated exosomes using mass spectrometry, gel electrophoresis, and Western blot, and we investigate the size, charge, and morphology of the exosomes using cryo-electron microscopy, dynamic light scattering (DLS), and ζ potential measurements. We then use this information to design simplified model systems that mimic different aspects of the exosomes, and we explore how they impact α -syn aggregation kinetics. Thus, we examine α -syn aggregation in the presence of exosomes from cells without or with overexpressed α -syn, either wild-type or disease-related mutant protein. We also investigate α -syn aggregation in the presence of artificial vesicles composed of exosome lipid extracts or models composed of biologically relevant lipids, including phosphatidylcholine (PC), anionic phosphatidylserine (PS, common lipid in outer leaflet of the cell plasma membranes), cardiolipin (CL, common in mitochondria), as well as neuro-specific GM1 and GM3 gangliosides and cationic sphingosine. Furthermore, we study the seeding effect by adding small amounts of α -syn fibril seeds. Most experiments are performed at mildly acidic pH to mimic the conditions in endosomes and lysosomes. Under these conditions, the aggregates seem to multiply due to secondary nucleation of monomers on fibrils, a process that is not detected at neutral pH (35).

EXPERIMENTAL PROCEDURES

Materials—The following lyophilized lipids were obtained from Avanti Polar Lipids (Alabaster AL): 1',3'-bis(1,2-dioleoyl-*sn*-glycero-3-phospho)-*sn*-glycerol sodium salt (cardiolipin,

CL); 1,2-dioleoyl-*sn*-glycero-3-phospho-L-serine sodium salt (DOPS); 1,2-dioleoyl-*sn*-glycero-3-phosphocholine (DOPC); D-erythrospingosine; and GM1 and GM3 ganglioside from ovine brain and milk, respectively. Buffer chemicals MES, NaCl, and ThT were of analytical grade, and the water used was ultra-pure (<18.2 megohms·cm at 25 °C, MilliQ grade).

α -Synuclein—Human α -syn was expressed in *Escherichia coli* from the aS-pT7-7 plasmid (kindly provided by Dr. H. Lashuel) and the monomer purified using ion exchange and gel filtration chromatography, as described previously (36), in buffer (10 mM MES, pH 5.5, with 140 mM NaCl, unless otherwise stated) just prior to setting up the kinetic measurements. The protein concentration was determined from the integrated area under the collected peak using the extinction coefficient $\epsilon_{280} = 5800 \text{ liters}\cdot\text{mol}^{-1}\cdot\text{cm}^{-1}$ or by measuring a UV absorbance spectrum from 350 to 220 nm, followed by baseline correction for light scattering effects to obtain the absorbance at 280 nm. The samples were prepared on ice, and 30 μM α -syn (0.4 mg/ml) was supplemented with 20 μM ThT to follow the fibrillation process. α -Syn was also studied in the absence and presence of 0.25 mg/ml exosomes (based on protein content) or 0.1–0.5 mM lipid in the form of small unilamellar vesicles (SUVs). The samples were aliquoted in 96-well plates (non-treated black polystyrene, full volume plates, 3631 Costar) and sealed with a plastic film to avoid evaporation. The pH was measured for all samples and found not to change due to the additions. For seeding experiments, 30 μM α -syn monomer was supplemented with 0.03 or 0.3 μM sonicated fibrils (*i.e.* 0.1 and 1%) counted as monomer equivalents. These fibrils were formed from 30 μM α -syn, collected directly after reaching the final ThT plateau, and sonicated briefly in a sonicator bath to disperse lumped fibrils. Experiments aimed at comparing the seeding efficiency between preformed seeds made in the absence and presence of 0.25 mg/ml exosomes were performed in 96-well plates with a nonbinding surface (black polystyrene plates treated with a pegylated surface, half-area, 3881 Corning Glass). These nonbinding plates were also used to explore the catalytic effect of SUVs composed with ganglioside lipids. Plates were incubated at 37 °C up to 144 h in a FLUOstar Omega or Galaxy plate reader under quiescent conditions or with shaking at 100 rpm between readings.

α -Synuclein Solubility—Samples at different time points were aliquoted and centrifuged for 10 min at $13,000 \times g$. The concentration of monomeric α -syn was monitored by UV absorbance at 280 nm for each supernatant, performing at least three measurements per sample, using the Thermo Scientific Nanodrop 2000 spectrophotometer. Specific time points during the lag phase, exponential growth phase, and at the plateau were selected for analysis. These time points were easily pinpointed by following in parallel well controlled and reproducible ThT aggregation kinetics.

Cell Culture and Cell Lines—Mouse neuroblastoma cells (N2a) were cultured in Dulbecco's modified Eagle's medium (DMEM) supplemented with 10% fetal calf serum, 100 units/ml penicillin, and 100 $\mu\text{g}/\text{ml}$ streptomycin. Cells were incubated in a humidified incubator set at 5% CO_2 and 37 °C. Plasmids used for α -syn overexpressing lines were described previously (37) with the exception that α -syn was tagged at the C-terminal end

with an HA tag. Mutant lines were generated by site-directed mutagenesis. For plasmid transfection, cells were transfected using TurboFect according to the manufacturer's protocol (Thermo Fisher), and stable lines were generated by growing and then maintaining cells in the presence of G418 at concentrations of 200 and 80 $\mu\text{g}/\text{ml}$, respectively.

Exosome Purification and Characterization—Exosomes were isolated from cell culture medium as described previously (38). Briefly, N2a cells were cultured for 48 h in serum-free DMEM. Collected medium was then depleted of cells and cellular debris by sequential low speed centrifugation. Exosomes were then isolated by centrifugation of the collected supernatant at $100,000 \times g$ at 4 °C for 90 min. The resultant pellet was then washed in PBS and centrifuged for 70 min at $100,000 \times g$ at 4 °C. Exosomes were analyzed for size using nanoparticle tracking analysis (NTA) and for purity by Western blotting. The concentration based on protein content was estimated by recording a UV absorbance spectrum from 350 to 220 nm, followed by baseline correction for light scattering effects to obtain the absorbance at 280 nm, and using an approximate absorbance coefficient of 1 liter $\text{g}^{-1} \text{cm}^{-1}$. The digestion of exosomes was performed as described previously (32), followed by Western blot analysis.

Western Blot—Cell or exosome pellets were lysed directly in Laemmli buffer and boiled for 10 min before samples were applied to 10–20% polyacrylamide gels (Bio-Rad) and subsequent transfer to PVDF membrane using Transblot Turbo transfer packs (Bio-Rad). Membranes were fixed in 0.4% paraformaldehyde (39) before blocking in 5% skim milk powder. The membranes were incubated in primary antibody (HA and Alix (Cell Signaling Technologies), Flotillin-1 (BD Transduction Laboratories), calnexin and GAPDH (Abcam)) solutions overnight. HRP-conjugated secondary antibodies were from Cell Signaling Technologies. Protein bands were detected using Signal Fire ECL reagent (Cell Signaling Technologies) and imaged on Bio-Rad ChemiDoc XRS+.

Vesicle Preparation—SUVs were prepared by sonication using a probe sonicator (Vibra-Cell, Sonics). Lipids were dissolved in $\text{CHCl}_3/\text{MeOH}$ 2:1 (v/v), and a thin film was formed by air-drying. Any residual solvent was evaporated in a vacuum chamber for at least 12 h. After adding buffer to a final concentration of 1 mM lipid, the samples were vortexed and then sonicated for 10 min using a pulsed sequence (10 s on and 10 s off at 70% amplitude) on ice. Any particulate matter from the probe was removed by 3 min of centrifugation at 13,000 rpm. Exosome lipids were extracted by the Blich-Dyer method (40), and the SUVs were prepared as above.

Light Scattering—DLS and ζ potential measurements were performed using a Malvern Zetasizer Nano ZS (Malvern Instruments, Malvern, UK) at 25 °C.

Nanoparticle Tracking Analysis—NTA, monitoring the Brownian motion of vesicles, was performed at room temperature using a NanoSight instrument (Malvern Instruments, Malvern, UK).

Cryogenic Transmission Electron Microscopy (cryo-TEM)—To ensure a stable temperature and avoiding loss of solution during sample preparation, a controlled environment vitrification system was used. Samples were prepared as thin liquid

films (<300 nm thick) on glow discharge-treated lacey carbon film-coated copper grids and plunged into liquid ethane at -180 °C. In this way, the original microstructures are preserved so that we can avoid component segmentation and rearrangement in addition to water crystallization as the samples are vitrified. Samples were stored under liquid N_2 until measured and then transferred using an Oxford CT3500 cryoholder and its workstation into the electron microscope (Philips CM120 Biotwin Cryo) equipped with a post-column energy filter (Gatan GIF100). An acceleration voltage of 120 kV was used, and images were recorded digitally with a CCD camera under low electron dose conditions.

Lipid Analysis—Extraction of the lipids from the isolated N2a exosomes was carried out by mixing 100 μl of the exosome suspension with 1 ml of $\text{CHCl}_3/\text{MeOH}$ (2:1) for 3 h at room temperature. The water phase was removed, and the organic phase was dried in a desiccator. Before being subjected to MS analysis, the dried samples were dissolved in 100 μl of $\text{CHCl}_3/\text{MeOH}$ (1:2) and mixed (1:1) with MeOH containing either 10 mM ammonium acetate or 0.4 mM methylamine, reaching a final concentration of either 5 mM ammonium acetate or 0.2 mM methylamine in $\text{CHCl}_3/\text{MeOH}$ (1:5).

Samples were analyzed using a nano-electrospray ionizer connected to an Orbitrap-Velos Pro mass spectrometer (Thermo Scientific, Waltham, MA). Samples (~ 2 μl) were loaded in disposable emitters and sprayed using negative ionization. Data were collected using data-dependent acquisition performing full scan experiments as well as untargeted MS/MS using higher energy collisional dissociation fragmentation. Relative intensities were calculated within each lipid class by averaging full scan spectra and for each lipid species using the isotope compositions yielding the three lowest masses. The intensities of closely adjacent lipids were compensated according to the theoretical isotopic distributions.

RESULTS

Exosome Characterization—Western blot analysis of the exosome preparations revealed that they were enriched for the exosomal proteins Flotillin-1 and Alix. Calnexin staining of the blots shows that the preparation is free of cellular contamination (Fig. 1A). Unlike Flotillin-1 and Alix, the level of α -syn in exosomes is not enriched, suggesting it is not a major protein component of these vesicles. To further confirm the presence of α -syn in exosomes, we digested the exosome sample with 0.25% (w/v) trypsin in the presence and absence of 0.1% (w/v) saponin (Fig. 1B). Significant proteolysis was observed when saponin was used to lyse the exosomes; however, the majority of α -syn was found to be protected from digestion in the absence of saponin suggesting α -syn is inside the exosomes. This is consistent with a predominantly cytosolic localization of α -syn in the cells from which the exosomes originate. It has also been reported that only a fraction of α -syn is secreted in association with exosomes (32, 41). To confirm this, cell culture medium was subjected to trichloroacetic acid precipitation after exosome isolation and subsequent Western blot analysis. In comparing the total amount of α -syn found associated with exosomes to that which remains in the culture media after exosome removal (Fig. 1C), we also find that only a minor component of total extracellular α -syn associates with exosomes.

Exosomes Catalyze α -Synuclein Aggregation

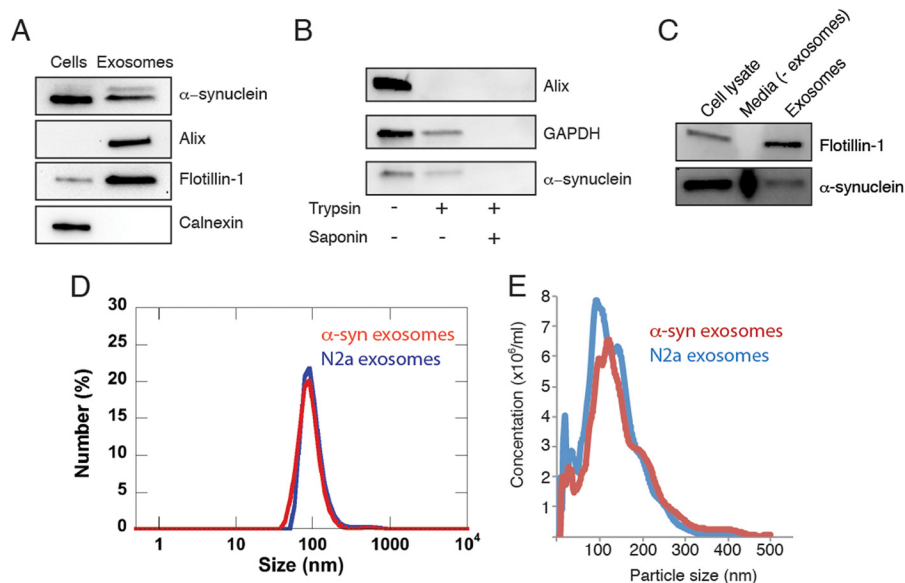


FIGURE 1. Characterization of exosomes. *A*, whole cell lysates and exosomes were subjected to Western blot analysis with antibodies against the proteins indicated. *B*, exosomes were treated with 0.25% trypsin \pm 0.1% saponin before Western blotting with antibodies against α -syn, GAPDH (cytosolic protein), and Alix (membrane protein). *C*, relative levels of α -syn in cell lysates compared with that secreted, either free or in exosomes, was analyzed by Western blotting. Cell lysate represents 1% of total cells; media (–exosomes) represents 10% of culture medium TCA-precipitated after exosome isolation, and 50% of total exosomes isolated were loaded. *D*, dynamic light scattering of exosomes from N2a cells with or without overexpressing-type α -syn shows vesicles of around 100 nm in diameter (analyzed by number). *E*, isolated exosomes from N2a cells (blue) or N2a cells overexpressing wild-type α -syn (red) were analyzed by NanoSight nanotracking analysis.

The size distribution in the exosome samples was determined using DLS and NTA. The main species in the DLS measurements, representing around 99% of the vesicles by number, was found to have a diameter around 100 nm, which is typical for exosomes (42), and the minor portion (<1%) has a considerably larger diameter (Fig. 1*D*). NTA showed similar results (Fig. 1*E*). The measured ζ potential for exosomes was similar to that obtained for small unilamellar vesicles (SUVs) with anionic lipids (Table 1). We can thus conclude that the exosomes are negatively charged. The cryo-TEM images of the exosomes show unilamellar, spherical vesicles with a diameter of 96 ± 8 (\pm S.E.), in agreement with the DLS and NTA measurements. Also, a fraction of larger exosomes was visible, with a diameter of 185 ± 35 nm (\pm S.E.). The membrane thickness was found to be 6 nm, which is typical for cell membranes (normally 4–10 nm) (43, 44). Exosomes from cells overexpressing human α -syn contain dark gray fields (Fig. 10*A*), which may represent protein or some other components of the exosomes. Additional exposure leads to blistering of these fields, further supporting a protein component. However, from these images alone, it is not possible to tell whether this is α -syn, another protein, or several proteins. The cryo-TEM images also show that the vesicles deform when they approach each other, consistent with electrostatic repulsion between the charged membranes.

Although we cannot rule out the influence of other extracellular vesicles, our analysis shows that the vesicles isolated meet the criteria for exosomes, and for this reason we will refer to the vesicles we isolated as exosomes. Unless otherwise stated, the term exosomes refers to exosomes isolated from N2a cells overexpressing wild-type α -syn.

Reproducible Kinetics Require a Defined Starting State—Central to all the kinetic studies in this investigation is our previously published study where we identified mild conditions

TABLE 1
 ζ potential of α -syn and SUVs used in the kinetic assays and cryo-TEM

Sample	ζ potential <i>mV</i>
α -syn exosomes	–16
6% CL SUVs	–21
30% DOPS SUVs	–27
100% DOPC SUVs	–0.5
15% sphingosine SUVs	21
10% GM1 SUVs	–11
α -syn monomers	–1.5
α -syn fibrils	–23

resulting in reproducible aggregation kinetics under quiescent conditions or with gentle shaking at slightly acidic pH (36). A key procedure to achieve reproducibility is the gel filtration step used to isolate monomeric protein in degassed buffer. This setup was used previously to explore α -syn interactions with lipids (36, 45) and in this study to characterize the effect of exosomes on α -syn aggregation rate. α -syn has been suggested to exist in a tetrameric state *in vivo*, although the relevance and existence of this form is debated (46, 47). Therefore, isolation of the monomer to obtain a well defined starting state may still be preferred for *in vitro* studies.

The aggregation experiments were performed in slightly acidic conditions. At neutral pH, the α -syn aggregation process is very slow, although it can be accelerated by the vigorous shaking or addition of beads or surfactants (48). When pH is reduced to pH 5.5, the aggregation occurs much faster and can also be reached without agitation (36). Indeed, the rate of secondary nucleation is dramatically increased at mildly acidic pH compared with neutral pH, which explains the acceleration of the aggregation process at the lower pH value (35). This difference in aggregation kinetics can be explained by the reduced electrostatic repulsion between protein units upon the change

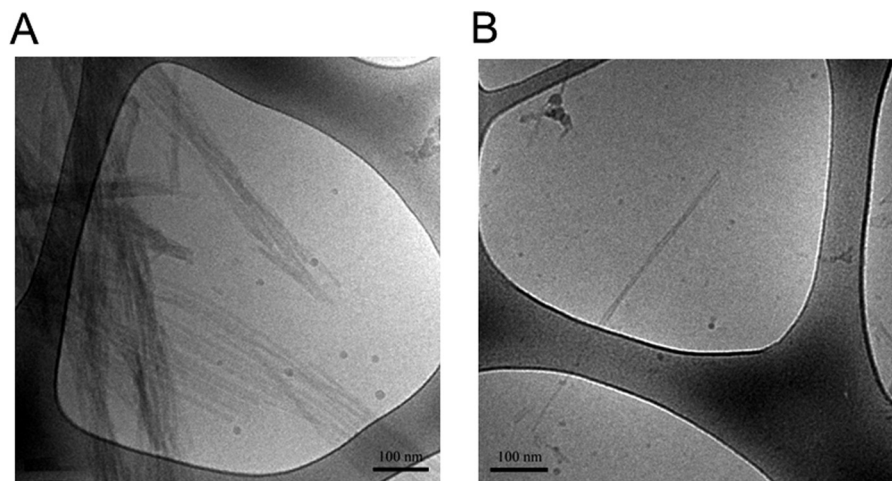


FIGURE 2. **Formation of α -syn fibrils.** 5 μ l of α -syn fibrils in 10 mM MES, pH 5.5, with 140 mM NaCl, unless otherwise stated) was added to the glow-discharged grid for cryo-TEM imaging. *A*, examples of typical α -syn fibrils formed at pH 5.5. *B*, example of a typical α -syn fibril formed at pH 7.5.

in pH. At pH 7, α -syn is negatively charged, and when pH is reduced to 5.5, the protein net charge is close to zero (predicted pI 4.74 based on amino acid sequence).

ζ potential measurements for monomeric α -syn in 10 mM MES buffer, 140 mM NaCl, pH 5.5, show very low electrophoretic mobility (Table 1), which imply an almost uncharged protein under these solution conditions. Corresponding measurements of fibrillar α -syn were also performed showing higher electrophoretic mobility in the same range as the SUV systems investigated (Table 1). Finally, the fibrils formed at different pH values were investigated by means of cryo-TEM. Fibrils formed from α -syn alone at pH 5.5 (Fig. 2*A*) and pH 7.5 (Fig. 2*B*) appear to be morphologically different, in that the fibrils formed at pH 5.5 are more abundant and bundled, and at pH 7.5 a more distinct inter-filament separation in each fibril is observed.

α -Synuclein Aggregation Kinetics in the Presence of Exosomes— α -syn amyloid formation was studied in the absence and presence of exosomes isolated from naive N2a cells or N2a cells overexpressing α -syn. Primary nucleation in solution is extremely slow for α -syn. Experiments in nonbinding plates can therefore only detect acceleration by vesicles. In plain polystyrene plates, the surface promotes nucleation (49). In these plates, we can also observe and discuss catalytic effects, although an observed retardation could arise from a direct effect on the protein or interference with surface nucleation. The aggregation kinetics were followed by ThT fluorescence. When the ThT dye binds to amyloid fibrils and oligomers, it enters a less polar environment, and its rotation is restricted. This gives rise to an increase in fluorescence emission at 482 nm when ThT is excited at 442 nm, but the quantum yield for bound ThT is very sensitive to the detailed fibril structure. The method does not provide direct molecular information, and whereas binding to fibrils dominate the observed signal, the specificity of ThT binding in the pathway of amyloid formation is still not completely understood (50). However, if care is taken in terms of optimized ThT concentration, and a starting point corresponding to monomeric samples in degassed buffers, it is possible to obtain highly reproducible data for the aggregation kinetics (36, 51, 52).

Examples of data on the kinetics of amyloid formation starting from 30 μ M monomeric α -syn in the absence and presence

of exosomes (0.25 mg/ml based on protein content) in 10 mM MES, 140 mM NaCl, pH 5.5, are shown in Fig. 3. We find that under these conditions, exosomes accelerate α -syn aggregation. There is no significant difference between exosomes isolated from naive N2a cells or those overexpressing α -syn (Fig. 3*A*). Furthermore, exosomes from cells that overexpress disease-related mutants of α -syn (A53T, A30P, and E46K) are found to accelerate the α -syn aggregation to the same extent (Fig. 3*B*). From these experiments, we conclude that the half-time for the α -syn aggregation, $t_{1/2}$, in the presence of exosomes is less than one-third of $t_{1/2}$ for α -syn alone. Here, $t_{1/2}$ is defined as the time point for half the maximal elevation of ThT fluorescence relative to baseline. We also observe that the presence of exosomes accelerates the aggregation of α -syn under quiescent conditions, albeit both the perturbed and unperturbed process is slower (Fig. 3*C*). The faster aggregation we observe under shaking conditions is attributed to fibril breakage.

To further elucidate the catalytic effect of exosomes, a dose dependence kinetic assay was performed using exosomes ranging in concentration from 0.03 to 0.25 mg/ml (Fig. 3*D*). At the lowest concentration, we observe a significant decrease in $t_{1/2}$. As increasing amounts of exosomes are added, the lag time is further reduced, but to only a minor extent (Fig. 3*E*), suggesting that the presence of very low amounts of exosomes is sufficient to catalyze α -syn fibril formation. We also investigated whether exosomes would lead to aggregation of β -synuclein (β -syn), a less aggregation prone homologue of α -syn. β -syn was incubated in the presence or absence of 0.25 mg/ml of exosomes. No aggregation was observed during the time frame of the experiment (Fig. 3*F*).

To confirm and complement the aggregation kinetics monitored by ThT fluorescence, we measured the α -syn monomer concentration during the aggregation process. Here, samples were collected at different time points from ongoing aggregation reactions in the absence and presence of exosomes and spun down, and the absorbance of the supernatant was measured at 280 nm. There is a close correspondence between monomer depletion and fibril formation, both in the absence and presence of exosomes (Fig. 4) implying that the dominating species in solution are monomer and fibrils at all times. More-

Exosomes Catalyze α -Synuclein Aggregation

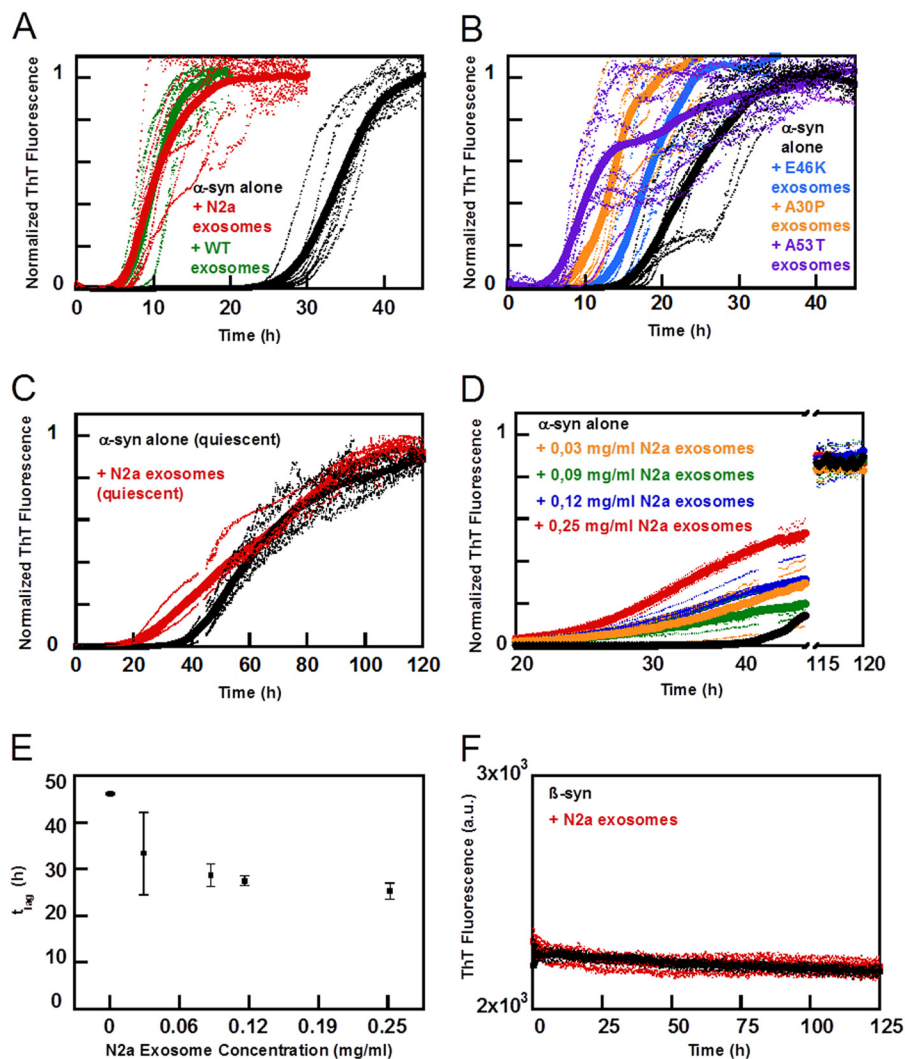


FIGURE 3. Aggregation kinetics of α -syn in the presence of exosomes. Aggregation kinetics for 30 μ M α -syn and β -syn was followed by ThT fluorescence in the presence and absence of exosomes in 10 mM MES, pH 5.5, with 140 mM NaCl. The averages of 4–8 replicate traces are shown in **boldface** with individual traces *dashed below*. *A*, aggregation of α -syn (black) with 0.25 mg/ml exosomes from N2a cells (red) or N2a cells overexpressing α -syn (green) show a distinct difference in lag time. Data were collected at 100 rpm. *B*, aggregation of α -syn (black) with 0.25 mg/ml exosomes from cells overexpressing disease-associated mutant α -syn (purple A53T, orange A30P, and light blue E46K) also exhibit a significantly shorter lag time than α -syn alone. Data were collected at 100 rpm. *C*, aggregation of α -syn (black) with 0.25 mg/ml exosomes from N2a cells (red) under quiescent conditions. *D*, dose dependence aggregation assay of α -syn in the presence of different exosome concentrations varying from 0–0.25 mg/ml. *E*, lag times, corresponding to 10% of maximum intensity, taken from the conditions depicted in *D* pointing again toward a significantly accelerated fibrillation when in the presence of exosomes. *F*, control experiment with β -syn, nonaggregating α -syn homologue protein, which remained unaffected in the presence of 0.25 mg/ml exosomes during the time frame assayed.

over, monomer is depleted earlier in the presence of exosomes, confirming the earlier formation of fibrils as deduced from the ThT measurements.

Exosome Lipid Composition—The MS analysis revealed the presence of several phospholipid classes in the exosomes, including PC, PS, PE, PI, and ganglioside classes GM2 and GM3, as summarized in Table 2 and supplemental Table S11. Within each class, we found several species with different fatty acids. The phospholipids were identified by several means. The class and fatty acid composition was determined by MS/MS, through characteristic fragmentation of the headgroup and fatty acids anions. The experimentally observed mass was found to lie within 5 ppm from the theoretical one. The PC lipids were detected as acetate adducts in samples using ammonium acetate, whereas most other lipids could be observed in either ammonium acetate or methylamine. The most abundant PS, PC, PI, and PE species contained 18:1, 18:0,

16:1, and 16:0 acyl chains. Other species were also detected having 20:0–4, 22:0–6, and 24:0–4 in combinations with 18:0–1 or 16:0–1 acyl chains.

Several species of ganglioside were found to have a characteristic fragment of sialic acid (Neu5Ac) with m/z 290.088. To investigate further, an additional experiment selecting such a lipid m/z 1354.8 for MS/MS using collision-induced dissociation fragmentation was performed. The mass spectrum of the fragments shows a consequential loss of Neu5Ac followed by *N*-acetylglucosamine (GlcNAc) and two hexoses (Hex), which indicate the identity of a GM2 species with a 16:0 acyl chain (Fig. 5). Similar experiments were also found the presence of several GM3 species. In Table 2, all the GM species found are shown with their relative abundance and class. The most abundant GM2 and GM3 species mostly contained saturated fatty acids, in which 16:0 was dominant (Table 2).

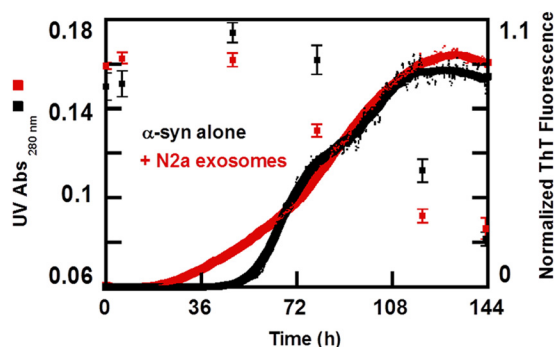


FIGURE 4. α -syn monomer concentration during the aggregation process. Normalized aggregation kinetics for $30 \mu\text{M}$ α -syn (black line) in the presence of 0.25 mg/ml exosomes (red line) followed by ThT fluorescence in 10 mM MES, pH 5.5, with 140 mM NaCl. The average traces are shown in bold. In parallel to the ongoing aggregation process, solubility changes of α -syn alone (black squares) and in the presence of 0.25 mg/ml exosomes (red squares) were monitored. Samples were collected at different stages of the aggregation profile and centrifuged, and absorbance measurements were performed to the supernatant. Each time point therefore represents an average value of at least three repeated absorbance measurements of soluble monomeric α -syn with respective standard deviation bar represented. Well depicted is the correlation between monomer depletion and fibril elongation in the presence and absence of exosomes.

TABLE 2

Phospholipid found in exosomes

Phospholipid classes detected are PE, PS, PI, PC, and the gangliosides GM2 and GM3. Fatty acid composition was determined from MS² in which relative intensity is calculated within each lipid class, and where 100% represents the most abundant species found; ppm denotes the deviation of the experimental value from the theoretical.

Class	Fatty acid	Lipid m/z/ppm	Relative intensity %
PE	18:1-16:0	716.5252/2.3	35
PE	18:1-18:1	742.5403/1.4	100
PE	18:1-18:0	744.556/1.5	42
PE	18:1-20:4	764.525/1.9	31
PE	18:0-20:4	766.5408/2.1	71
PE	18:0-20:3	768.5562/1.7	51
PS	16:0-18:1	760.5142/1.0	32
PS	18:1-18:1	786.53/1.2	24
PS	18:1-18:0	788.5454/0.9	100
PS	18:0-20:4	810.5278/-1.5	21
PS	18:1-22:0	844.6096/2.7	67
PI	18:1-18:1	861.5509/1.2	71
PI	18:0:18:1	863.5665/1.2	100
PI	18:0-20:4	885.5516/2.0	36
PI	18:0-20:3	887.5667/1.4	93
PI	18:0-20:2	889.582/1.0	57
PC	16:0-16:2	788.5456/1.1	50
PC	16:0-16:1	790.5606/0.3	21
PC	16:0-16:0	792.5767/0.9	20
PC	16:0-18:1	818.5914/-0.3	100
PC	18:1-18:0	846.6242/1.5	50
GM3	16:0	1151.7080/1.9	52
GM3	20:0	1207.7705/1.7	7
GM3	22:0	1235.8017/1.5	9
GM3	24:1	1261.8172/1.4	12
GM3	24:0	1263.8325/1.1	16
GM2	16:0	1354.7880/2.0	100
GM2	18:0	1382.8184/1.3	8
GM2	20:0	1410.8500/1.5	12
GM2	22:0	1438.8826/2.4	21
GM2	24:1	1464.8972/2.1	31
GM2	24:0	1466.9118/0.9	34

α -Synuclein Aggregation Kinetics in the Presence of Model Membranes—The aggregation kinetics of α -syn was studied in the absence and presence of SUVs prepared from defined lipid mixtures (Fig. 6, A–C) or from lipid extracts of exosomes (Fig.

6D). α -syn aggregation is accelerated by the exosome lipid SUVs in a similar manner as observed with intact exosomes. This supports the notion that exosome lipid constituents play a role in the observed acceleration. However, most of the model lipid SUVs of similar size that we investigated did not accelerate α -syn aggregation, irrespective of lipid charge. Fig. 6, A–C, shows representative aggregation kinetics data for α -syn in the presence of SUVs composed of pure DOPC (uncharged, zwitterionic), DOPC with 6 mol % CL (net charge -2) (53), DOPC with 30 mol % DOPS (net charge -1), or DOPC with 15 mol % sphingosine (net charge $+1$). α -syn aggregation is not accelerated by any of these lipid systems, and in some cases we instead observe a minor retardation (Fig. 6, A–C). Thus, charge alone does not explain the acceleration of α -syn aggregation caused by the exosomes.

Effect of Lipid Concentration on α -Synuclein Aggregation Kinetics—Using a standard phosphorous assay (54), we estimated the lipid content in the exosome samples to 0.6 mM total lipids for exosome samples with total protein concentration (based on A_{280}) of 1 mg/ml . The exosome concentration used in the aggregation assays then corresponds to $\sim 0.15 \text{ mM}$ total lipid. Because this estimate cannot be considered to be very precise, we performed aggregation experiments with several concentrations of model vesicles (Fig. 7, A and B). This was done to investigate the role of available amounts of lipids or vesicle surface in the sample. We find that the lipid/protein ratio governs the effect on aggregation. At low lipid/protein ratios, the lag time is not significantly altered in the presence of DOPC, DOPS, or CL SUVs, although there is retardation in all lipid/protein ratios investigated with the stronger effect at higher lipid concentrations (Fig. 7A). In contrast, SUVs made of extracted exosome lipids accelerate aggregation except at the highest concentration where we did not observe any aggregation (Fig. 7B). Thus, under the present experimental conditions, none of the common membrane lipids DOPC, DOPS, or CL vesicles cause any acceleration at any concentration investigated, suggesting that other lipid species in the vesicles prepared from exosome-derived lipids are involved.

α -Synuclein Aggregation Kinetics in the Presence of Ganglioside Membranes—The lipid analysis of isolated exosomes identified ganglioside classes GM2 and GM3. We therefore studied α -syn aggregation kinetics in the presence of model vesicles that include gangliosides. GM2 is not commercially available and could therefore not readily be investigated; however, both GM3 and GM2 are truncations of GM1, and as the three species have similar structures, we therefore studied aggregation kinetics in the presence of GM1 and GM3. Vesicles composed of DOPC with 10 mol % of GM3 or GM1 were prepared, and the effect of these vesicles on α -syn aggregation kinetics was investigated (Fig. 8, A–C). In sharp contrast to all other model lipid systems studied here (Figs. 6, A–C, and 7), the addition of these vesicles to the monomeric recombinant α -syn was found to accelerate the aggregation process in a concentration-dependent manner. All samples containing vesicles at 0.5 mM total lipid concentration exhibited faster aggregation than the samples containing vesicles at 0.2 mM total lipid concentration, which in turn aggregate faster than samples containing α -syn alone (Fig. 8, A–C). Clearly, vesicles composed of GM1 pro-

Exosomes Catalyze α -Synuclein Aggregation

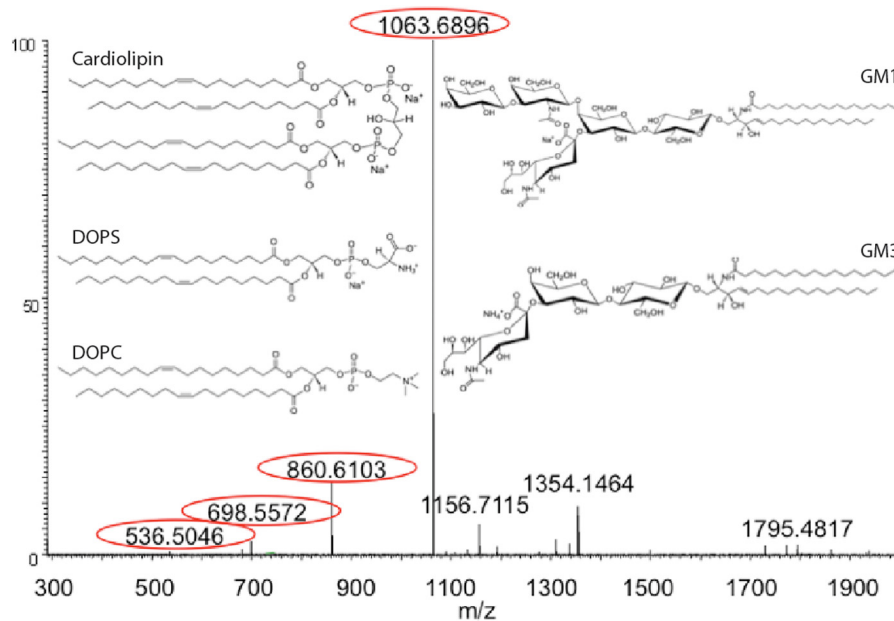


FIGURE 5. **Lipid identification by mass spectrometry.** Fragmentation of GM species m/z 1354.8 with a neutral loss of Neu5Ac (-291.1), Neu5Ac + GlcNAc (-494.2), Neu5Ac + GlcNAc + Hex (-656.2), and Neu5Ac + GlcNAc + 2Hex (-818.3) marked in circles. Insets show lipid structures as indicated.

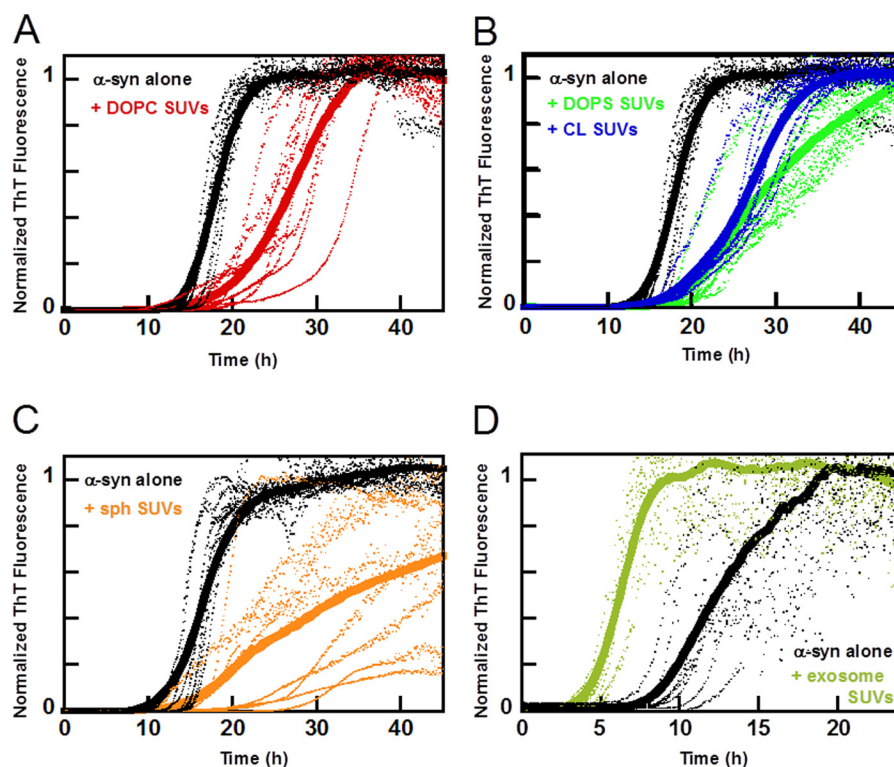


FIGURE 6. **Aggregation kinetics of α -syn in the presence of SUVs.** Aggregation kinetics for α -syn was measured by ThT fluorescence in the presence of SUVs in 10 mM MES, pH 5.5, with 140 mM NaCl. The averages of eight replicate traces are shown in **bold** with individual traces *dashed* below. *A*, aggregation of $30 \mu\text{M}$ α -syn (*black*) with 0.2 mM DOPC SUVs (*red*). *B*, aggregation of $30 \mu\text{M}$ α -syn (*black*) with 0.2 mM 30% DOPS SUVs (*green*) or 0.2 mM 6% cardiolipin SUVs (*blue*). *C*, aggregation of $30 \mu\text{M}$ α -syn (*black*) with 0.2 mM 15% sphingosine SUVs (*orange*). All mixtures are based on DOPC with addition of the indicated lipid. In all instances, the aggregation is retarded or shows no significant change in lag time when the lipid vesicles are added. *D*, aggregation of $30 \mu\text{M}$ α -syn alone (*black*) with extracted exosome lipid SUVs (*green*). Addition of SUVs made from extracted exosome lipids was the only model system studied that catalyzed the aggregation kinetics of α -syn.

mote aggregation of α -syn also in nonbinding pegylated plates (Fig. 8B), where α -syn alone does not aggregate during the time frame acquired.

Aggregation in the Presence of Pre-formed Seeds—The addition of seeds composed of pre-formed amyloid fibrils is one

efficient way to accelerate aggregation, due to secondary nucleation being favored at mildly acidic pH (35). Therefore, we compared the acceleration of amyloid formation observed with exosomes with that obtained with controlled amounts of seeds. Consequently, we studied the aggregation kinetics for samples

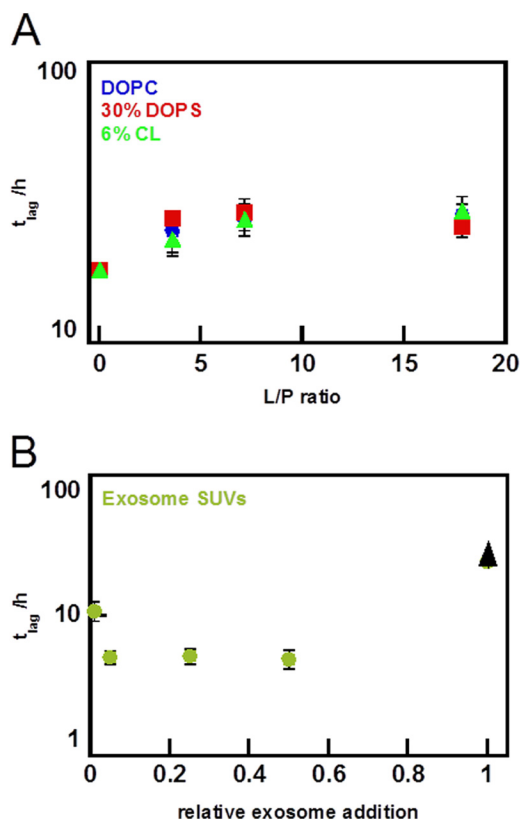


FIGURE 7. Effect of lipid to protein ratio on aggregation lag time. $30 \mu\text{M}$ α -syn was incubated in the presence of different concentrations of SUVs in 10 mM MES, pH 5.5, with 140 mM NaCl. The lag time is defined as the time when 10% of the maximum intensity is reached, and the error bars represent the standard deviation from eight replicates. All mixtures are based on DOPC with addition of the indicated lipid. *A*, lag time dependence for varying lipid to protein ratio for pure DOPC SUVs (blue), 30% DOPS SUVs (red), and 6% cardiolipin SUVs (green). Data collected at 100 rpm. *B*, lag time dependence for varying lipid to protein ratio for SUVs made from exosome lipids reported in relative lipid ratio. Addition of exosome SUVs decrease lag times until a threshold is reached and where the aggregation does not start within the experimental time frame (black arrowhead). Data were collected at 100 rpm.

that contain (at time 0) $30 \mu\text{M}$ α -syn monomer complemented with 0, 0.03, or $0.3 \mu\text{M}$ preformed α -syn fibrils (counted as monomer equivalents; Fig. 8D). At these low amounts of seeds (0.1 and 1%), elongation would be below the noise level of the ThT experiment. These small amounts of seeds are found to shorten the lag phase in a reproducible manner indicative of secondary nucleation of monomers on the fibril surface (44). In the presence of 1% seeds, the half-time has decreased by around 40% relative to the unseeded case. This reduction is slightly smaller than the reduction we observed for the samples containing exosomes.

We also studied whether seeds formed in the presence of exosomes have the same seeding efficiency as those formed in the absence of exosomes (Fig. 9). No discernable difference between the two seeds was observed.

Morphology of α -Synuclein Aggregates in the Presence of Exosomes and Vesicles—The cryo-TEM images of exosomes from cells overexpressing α -syn show small dark patches in the membrane and a small number of gray features in or around the exosomes when imaged directly after isolation (Fig. 10A). When recombinant α -syn is mixed with exosomes, there is an immediate increase in the number of gray patches around exo-

somes in the cryo-TEM images (Fig. 10B). After incubating the exosomes with recombinant α -syn for 18 h, fibrils are also observed in the sample (Fig. 10C). There is no striking difference in morphology between fibrils formed in the absence and presence of exosomes (Figs. 2B and 10C). Interestingly, the fibrils are observed in the same areas as the exosomes (Fig. 10C). Similar behavior is seen when α -syn is incubated with SUVs that contain anionic lipids (6 mol % CL) (data not shown). In the latter case, the α -syn fibrils entwine the SUVs and twist along the membrane surface. Incubating recombinant α -syn with exosomes leads to more prominent patches in the exosome membrane that are darker than the surrounding membrane (Fig. 10D). These patches may contain protein, protein aggregates, or some other components. Interestingly, when recombinant α -syn is incubated with exosomes at neutral pH 7.5 instead of pH 5.5, we observe a “surface decoration” of the exosome membrane (Fig. 10E).

DISCUSSION

Exosomes Accelerate Aggregation—Exosomes have been suggested to play a role in the transfer of α -syn between neurons, contributing to the spread of PD pathology between brain regions (27, 30–33). The results of our study show that aggregation of exogenous α -syn is accelerated by exosomes irrespective of whether they are derived from control cells or cells overexpressing α -syn (Fig. 3). Our results lead us to further suggest that the lipid composition of the exosomes is crucial for the aggregation process.

Lipid or Protein Component?—The acceleration of α -syn aggregation (Fig. 3A) might be caused by the exosome lipid or protein components or by some additional factor in the exosome samples. To distinguish between these possibilities, we studied the aggregation kinetics starting from monomeric α -syn samples supplemented with SUVs prepared from lipids extracted from the exosomes (Fig. 6D). Both N2a cell-derived exosomes and SUVs made of exosome lipids were found to accelerate α -syn aggregation. This implies that exosome lipids are sufficient for acceleration of α -syn aggregation and that the protein components of exosomes are not necessary for this effect to arise.

The observed kinetics are sensitive to the ratio of lipid to protein (Fig. 7). In our experiments, we had a molar excess of lipids to protein ranging from 4 to 18 lipids per protein molecule or 2 to 9 lipids per protein counting the outer leaflet only (most vesicles are unilamellar, Fig. 9) (55). An area of 72 \AA^2 per DOPC headgroup (56) gives $100\text{--}700 \text{ \AA}^2$ membrane surface area per protein molecule, which is less than the cross-section area of around 900 \AA^2 for a globular protein of 14 kDa and is significantly less than the area of unfolded α -syn monomer (57, 58) or α -syn with partial helical structure as in the proposed binding model (59). Thus, all protein may not adsorb in a single layer. This is in agreement with the findings of surface catalysis by nanoparticles when the protein is in excess over available surface area (60).

Membrane Charge and Lipid Composition—SUVs of similar size as the exosomes were prepared from pure lipids with variation of charge and lipid headgroup in a systematic manner. The lipids PC, PS, CL, and sphingosine were chosen for their

Exosomes Catalyze α -Synuclein Aggregation

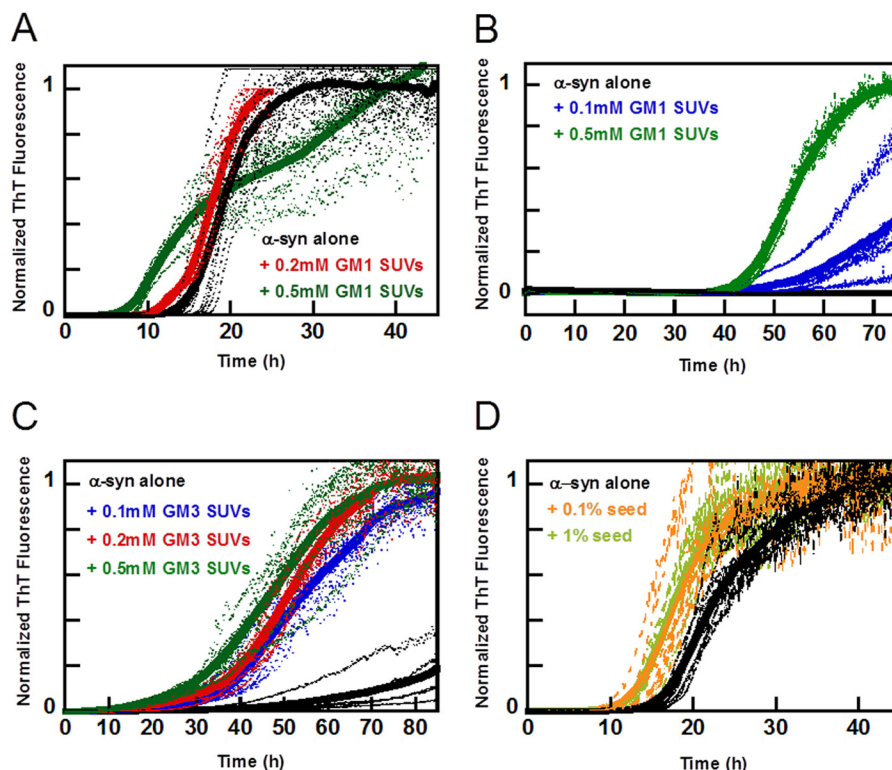


FIGURE 8. Aggregation kinetics of α -syn in the presence of ganglioside SUVs or α -syn seeds. Aggregation kinetics for α -syn was measured by ThT fluorescence in the presence of SUVs or α -syn seeds in 10 mM MES, pH 5.5, with 140 mM NaCl. The averages of eight replicate traces are shown in *bold* with individual traces *dashed* below. All mixtures are based on DOPC with addition of the indicated lipid. *A*, aggregation of α -syn (*black*) with 0.2 mM 10% GM1 SUVs (*red*) or 0.5 mM 10% GM1 (*green*) at 100 rpm. The biphasic behavior observed for 0.5 mM 10% GM1 SUVs is not reproduced in every experiment and may be due to the after-reaction of the formed fibrils (bundling and sedimentation, etc.) that perturbs the ThT fluorescence. *B*, aggregation of α -syn (*black*) with 0.1 mM 10% GM1 SUVs (*blue*) or 0.5 mM 10% GM1 (*green*) under quiescent conditions and in 96-well nonbinding pegylated surface plates. *C*, aggregation of α -syn (*black*) with 0.1 mM (*blue*), 0.2 mM (*red*), or 0.5 mM 10% GM3 SUVs (*green*) at quiescent conditions. *D*, aggregation of α -syn (*black*) with 0.1% (*orange*) or 1% seeds (*light green*) at 100 rpm.

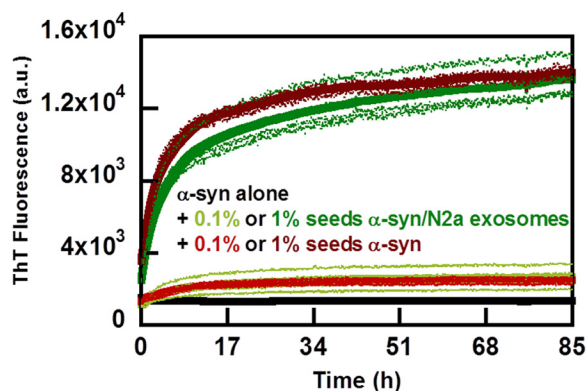


FIGURE 9. Aggregation kinetics with seeds formed in the presence or absence of exosomes. Aggregation of α -syn (*black*) was measured by ThT fluorescence in 10 mM MES, pH 5.5, with 140 mM NaCl in the presence of 0.1 or 1% seeds formed either with (*shades of green*) or without (*shades of red*) exosomes. The averages of four replicate traces are shown in *bold* with individual traces *dashed* below. Data were collected under quiescent conditions and in nonbinding pegylated surface plates.

biological relevance. PC is the most abundant lipid component of biological membranes, and the negatively charged CL and PS are relevant in PD and found in mitochondrial and plasma membranes. The amount of α -syn associated with mitochondria is increased in the substantia nigra of PD patients, and mitochondrial dysfunction is linked to PD pathogenesis (61). In addition to this, locally reduced pH occurs in mitochondria as a result of oxidative or metabolic stress (63), conditions relevant

for PD. An acidic environment is also present in the endosomal-lysosomal pathway (62), which, as mentioned earlier, is heavily implicated in PD. Exosomes have been shown to be taken up by endocytosis (64) and as such are exposed to the acidic environments utilized in this study. Model vesicles containing negatively charged lipids were prepared to have similar charge density and ζ potential as the exosomes. We also tested model membranes with cationic lipids, although α -syn is known to preferentially interact with anionic lipids (65–67). Positively charged sphingosine is a sphingolipid precursor of cell signaling molecules such as ceramides and sphingosine phosphate (68). None of the model vesicles tested induce acceleration of α -syn aggregation (Fig. 6, A–C), in contrast to exosomes and SUVs prepared from exosome lipids, and both significantly accelerated α -syn aggregation (Figs. 1 and 6D). Vesicle charge seems to be of minor importance to the aggregation kinetics at the investigated concentrations and solution conditions. Thus, the mere presence of a phospholipid membrane is not sufficient to accelerate α -syn aggregation, irrespective of membrane charge.

Ganglioside Lipids—The lipid analysis of exosome extracts identified ganglioside lipids. Interestingly, the acceleration of α -syn aggregation as observed in the presence of exosomes is reproduced by vesicle preparations composed of fluid lipid bilayers that contain ganglioside lipids GM1 or GM3. The observed acceleration of α -syn aggregation in the presence of exosomes might thus be attributed to the lipid components

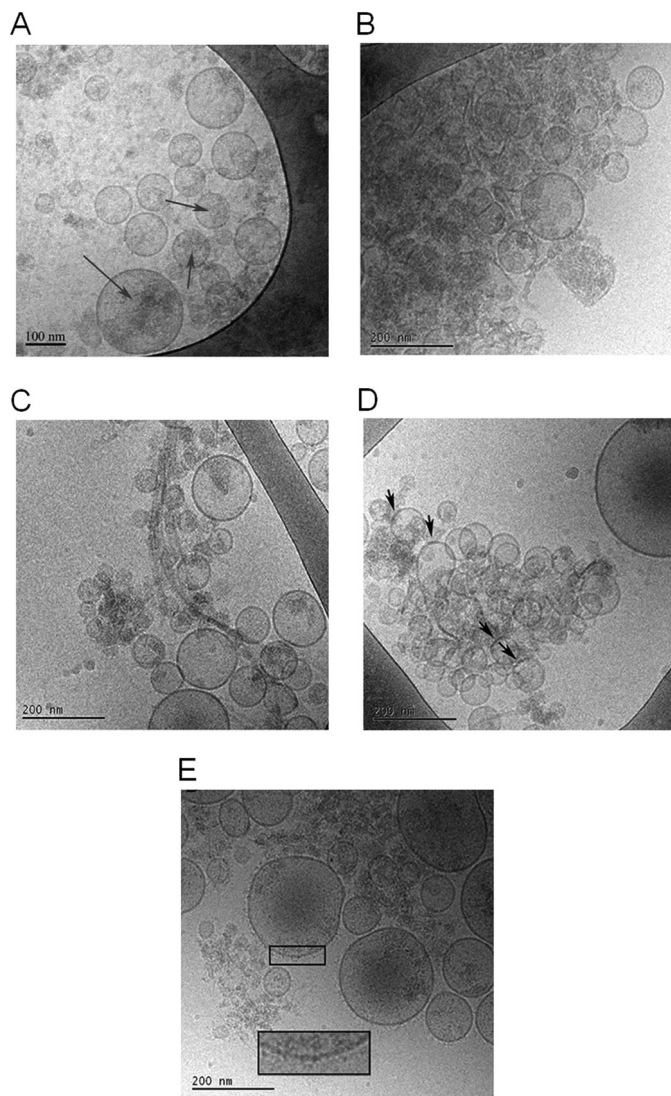


FIGURE 10. cryo-TEM analysis of fibrils. 5 μ l of α -syn fibrils formed in 10 mM MES, pH 5.5, with 140 mM NaCl was added to the glow-discharged grid for cryo-TEM imaging. *A*, exosomes isolated from N2a cells overexpressing wild-type α -syn reveal spherical unilamellar vesicles with the presence of darker gray areas inside and on top of the vesicles (exemplified by arrow). *B*, when recombinant α -syn is mixed with exosomes from cells overexpressing α -syn, an immediate increase in "gray shadows" appears in the same area of the grid as where exosomes are found. *C*, after 18 h of co-incubation of recombinant α -syn with exosomes from cells overexpressing wild-type α -syn fibrils associated with the exosomes are present. *D*, incubation of recombinant α -syn with the exosomes leads to formation of patches in the exosome membrane that are darker than the surrounding membrane (marked by arrows). *E*, incubation of recombinant α -syn with exosomes overexpressing α -syn at neutral pH 7.5. Here a surface decoration of the exosome membrane is observed (inset shows magnification).

GM2 and GM3, which are both truncated versions of GM1. Accelerated aggregation by ganglioside membranes has been observed for amyloid β ($A\beta$) from Alzheimer disease (AD) and islet amyloid polypeptide from diabetes type II (69–71). The opposite effect has been reported for α -syn, pH 7.5, in the presence of lipid model membranes containing ganglioside (57). This may be due to the difference in pH, lipid phase behavior (fluidity and domain formation) or other variations of the experimental setup. For example, the protein-to-lipid ratio, protein-to-surface area ratio, convection, and differences in

surface material of the measuring cells, have all been shown to strongly affect α -syn surface nucleation (60).

Molecular Mechanism—Our results clearly show that the presence of exosomes affects the aggregation process and that the lipid composition is critical for the magnitude and nature of the effect. The underlying molecular mechanisms seem to rely on protein interaction with the lipid membrane. Still, many details remain elusive, and several scenarios might explain our observations. (i) Accumulation of protein at the bilayer interface may lead to surface catalysis and accelerated aggregation (60, 72). (ii) The adsorbed protein may bury hydrophobic segments in the apolar region of the bilayer, influencing the interactions with other protein molecules, and this may lead to catalysis or retardation of aggregation. (iii) Protein-lipid co-aggregation is another possible scenario that can lead to acceleration and retardation of the aggregation process. (iv) Protein adsorption to negatively charged ganglioside-containing membranes with large oligosaccharide headgroups might occur in a different manner compared with lipid bilayers with PS or CL where α -syn penetrates into interfacial headgroup region (45, 73). Lower acyl chain exposure may reduce the degree of protein penetration into the hydrophobic region of the membrane leading to conditions where surface catalysis is enhanced on ganglioside membranes.

Secondary Nucleation—In the seeding experiment, we observe a shortening of the lag phase, which indicates that the aggregation process is amplified by secondary nucleation, presumably of monomers on the fibril surface. This provides an autocatalytic feedback loop as recently found for $A\beta$ (52, 74, 75). The α -syn aggregation process is highly pH-sensitive. At neutral pH under quiescent conditions, α -syn aggregation is extremely slow, and at mildly acidic pH (below pH 6), the rate of secondary nucleation increases dramatically, leading to much faster overall aggregation (35), presumably due to charge neutralization of monomer or fibril.

Exosomes and Other Amyloid Proteins—The interaction of another neurodegenerative disease-associated protein, $A\beta$, with gangliosides is well established (69, 76), and elevated ganglioside concentration is found in the brain and cerebrospinal fluid (CSF) of AD patients. Ganglioside-bound $A\beta$ has been identified in CSF (77, 78) and is believed to be involved in seeding of amyloid fibrils in AD (70, 77, 79). Exosomes are suggested to play a role in AD pathogenesis, and ganglioside-containing fibrils are inferred to be toxic to cells (80, 81). Furthermore, in a mouse model of Sandhoff disease, a lysosomal disorder characterized by accumulation of GM2, it was observed that $A\beta$ accumulated in the brains of these mice, whereas α -syn was accumulated in the substantia nigra (82). Lysosomal dysfunction is believed to play a role in PD (83, 84) and has been shown to enhance both α -syn and exosome secretion (32, 33, 41). In this study, we show that exosomes enhance the aggregation of α -syn, and this may be one factor inducing aggregation of extracellular α -syn. Given the role of these vesicles in transferring protein between cells, this then represents a viable pathway for spreading α -syn pathology in the PD brain. Indeed, this idea is supported by a recent study that shows monomeric Tau aggregated in endosomal components (85). Based on this, we may speculate that extracellular α -syn would interact with exosomes before being endocytosed; thereafter, it would encounter

Exosomes Catalyze α -Synuclein Aggregation

the acidic microenvironments of the endosomal pathway thus facilitating enhanced aggregation. Although we observed no enrichment of secreted α -syn on exosomes, the exosomes have a profound catalytic effect on α -syn aggregation kinetics, which we ascribe to the ganglioside lipid components. This, together with the autocatalytic multiplication of aggregates provided by the secondary nucleation at mildly acidic pH, provides important pieces of information in the complex puzzle of how α -syn interacts with biological membranes to promote neurological disease.

Acknowledgments—We thank Gunnel Karlsson for expert help with cryo-TEM and Karin Schillén for helpful discussions on DLS measurements.

REFERENCES

- Chivet, M., Hemming, F., Pernet-Gallay, K., Fraboulet, S., and Sadoul, R. (2012) Emerging role of neuronal exosomes in the central nervous system. *Front. Physiol.* **3**, 145
- Bonini, N. M., and Giasson, B. I. (2005) Snaring the function of α -synuclein. *Cell* **123**, 359–361
- Murphy, D. D., Rueter, S. M., Trojanowski, J. Q., and Lee, V. M. (2000) Synucleins are developmentally expressed, and α -synuclein regulates the size of the presynaptic vesicular pool in primary hippocampal neurons. *J. neurosci.* **20**, 3214–3220
- Cremades, N., Cohen, S. I., Deas, E., Abramov, A. Y., Chen, A. Y., Orte, A., Sandal, M., Clarke, R. W., Dunne, P., Aprile, F. A., Bertocini, C. W., Wood, N. W., Knowles, T. P., Dobson, C. M., and Klenerman, D. (2012) Direct observation of the interconversion of normal and toxic forms of α -synuclein. *Cell* **149**, 1048–1059
- Schapira, A. H. (2009) Neurobiology and treatment of Parkinson's disease. *Trends Pharmacol. Sci.* **30**, 41–47
- Graham, J. M., and Sagar, H. J. (1999) A data-driven approach to the study of heterogeneity in idiopathic Parkinson's disease: identification of three distinct subtypes. *Movement Disorders* **14**, 10–20
- Halliday, G. M., Holton, J. L., Revesz, T., and Dickson, D. W. (2011) Neuropathology underlying clinical variability in patients with synucleinopathies. *Acta Neuropathol.* **122**, 187–204
- Halliday, G. M., Ophof, A., Broe, M., Jensen, P. H., Kettle, E., Fedorow, H., Cartwright, M. I., Griffiths, F. M., Shepherd, C. E., and Double, K. L. (2005) α -Synuclein redistributes to neuromelanin lipid in the substantia nigra early in Parkinson's disease. *Brain* **128**, 2654–2664
- Harrower, T. P., Michell, A. W., and Barker, R. A. (2005) Lewy bodies in Parkinson's disease: protectors or perpetrators? *Exp. Neurol.* **195**, 1–6
- Wakabayashi, K., Tanji, K., Mori, F., and Takahashi, H. (2007) The Lewy body in Parkinson's disease: molecules implicated in the formation and degradation of α -synuclein aggregates. *Neuropathology* **27**, 494–506
- Winner, B., Jappelli, R., Maji, S. K., Desplats, P. A., Boyer, L., Aigner, S., Hetzer, C., Loher, T., Vilar, M., Campioni, S., Tzitzilonis, C., Soragni, A., Jessberger, S., Mira, H., Consiglio, A., Pham, E., Masliah, E., Gage, F. H., and Riek, R. (2011) *In vivo* demonstration that α -synuclein oligomers are toxic. *Proc. Natl. Sci. Acad. U.S.A.* **108**, 4194–4199
- Bucciantini, M., Giannoni, E., Chiti, F., Baroni, F., Formigli, L., Zurdo, J., Taddei, N., Ramponi, G., Dobson, C. M., and Stefani, M. (2002) Inherent toxicity of aggregates implies a common mechanism for protein misfolding diseases. *Nature* **416**, 507–511
- Lashuel, H. A., Overk, C. R., Oueslati, A., and Masliah, E. (2013) The many faces of α -synuclein: from structure and toxicity to therapeutic target. *Nat. Rev. Neurosci.* **14**, 38–48
- Chandra, S., Chen, X., Rizo, J., Jahn, R., and Südhof, T. C. (2003) A broken α -helix in folded α -synuclein. *J. Biol. Chem.* **278**, 15313–15318
- Eliezer, D., Kutluay, E., Bussell, R., Jr., and Browne, G. (2001) Conformational properties of α -synuclein in its free and lipid-associated states. *J. Mol. Biol.* **307**, 1061–1073
- Bussell, R., Jr., and Eliezer, D. (2003) A structural and functional role for 11-mer repeats in α -synuclein and other exchangeable lipid binding proteins. *J. Mol. Biol.* **329**, 763–778
- Robotta, M., Braun, P., van Rooijen, B., Subramaniam, V., Huber, M., and Drescher, M. (2011) Direct evidence of coexisting horseshoe and extended helix conformations of membrane-bound α -synuclein. *Chem. Phys. Chem.* **12**, 267–269
- Uversky, V. N. (2007) Neuropathology, biochemistry, and biophysics of α -synuclein aggregation. *J. Neurochem.* **103**, 17–37
- Chartier-Harlin, M. C., Kachergus, J., Roumier, C., Mouroux, V., Douay, X., Lincoln, S., Levecque, C., Larvor, L., Andrieux, J., Hulihan, M., Waucquier, N., Defebvre, L., Amouyel, P., Farrer, M., and Destée, A. (2004) α -Synuclein locus duplication as a cause of familial Parkinson's disease. *Lancet* **364**, 1167–1169
- Krüger, R., Kuhn, W., Müller, T., Woitalla, D., Graeber, M., Kösel, S., Przuntek, H., Epplen, J. T., Schöls, L., and Riess, O. (1998) Ala30Pro mutation in the gene encoding α -synuclein in Parkinson's disease. *Nat. Genet.* **18**, 106–108
- Polymeropoulos, M. H., Lavedan, C., Leroy, E., Ide, S. E., Dehejia, A., Dutra, A., Pike, B., Root, H., Rubenstein, J., Boyer, R., Stenroos, E. S., Chandrasekharappa, S., Athanassiadou, A., Papapetropoulos, T., Johnson, W. G., Lazzarini, A. M., Duvoisin, R. C., Di Iorio, G., Golbe, L. I., and Nussbaum, R. L. (1997) Mutation in the α -synuclein gene identified in families with Parkinson's disease. *Science* **276**, 2045–2047
- Singleton, A. B., Farrer, M., Johnson, J., Singleton, A., Hague, S., Kachergus, J., Hulihan, M., Peuralinna, T., Dutra, A., Nussbaum, R., Lincoln, S., Crawley, A., Hanson, M., Maraganore, D., Adler, C., Cookson, M. R., Muentner, M., Baptista, M., Miller, D., Blancato, J., Hardy, J., and Gwinn-Hardy, K. (2003) α -Synuclein locus triplication causes Parkinson's disease. *Science* **302**, 841
- Zarranz, J. J., Alegre, J., Gómez-Esteban, J. C., Lezcano, E., Ros, R., Ampuero, I., Vidal, L., Hoenicka, J., Rodriguez, O., Atarés, B., Llorens, V., Gomez Tortosa, E., del Ser, T., Muñoz, D. G., and de Yebenes, J. G. (2004) The new mutation, E46K, of α -synuclein causes Parkinson and Lewy body dementia. *Ann. Neurol.* **55**, 164–173
- Angot, E., Steiner, J. A., Hansen, C., Li, J. Y., and Brundin, P. (2010) Are synucleinopathies prion-like disorders? *Lancet Neurol.* **9**, 1128–1138
- Dunning, C. J., George, S., and Brundin, P. (2013) What's to like about the prion-like hypothesis for the spreading of aggregated α -synuclein in Parkinson disease? *Prion* **7**, 92–97
- Ximerakis, M., Pampalakis, G., Roumeliotis, T. I., Sykioti, V. S., Garbis, S. D., Stefanis, L., Sotiropoulou, G., and Vekrellis, K. (2014) Resistance of naturally secreted α -synuclein to proteolysis. *FASEB J.* **28**, 3146–3158
- Emmanouilidou, E., Melachroinou, K., Roumeliotis, T., Garbis, S. D., Ntzouni, M., Margaritis, L. H., Stefanis, L., and Vekrellis, K. (2010) Cell-produced α -synuclein is secreted in a calcium-dependent manner by exosomes and impacts neuronal survival. *J. Neurosci.* **30**, 6838–6851
- Bellingham, S. A., Guo, B. B., Coleman, B. M., and Hill, A. F. (2012) Exosomes: vehicles for the transfer of toxic proteins associated with neurodegenerative diseases? *Front. Physiol.* **3**, 124
- Dunning, C. J., Reyes, J. F., Steiner, J. A., and Brundin, P. (2012) Can Parkinson's disease pathology be propagated from one neuron to another? *Prog. Neurobiol.* **97**, 205–219
- Chang, C., Lang, H., Geng, N., Wang, J., Li, N., and Wang, X. (2013) Exosomes of BV-2 cells induced by α -synuclein: important mediator of neurodegeneration in PD. *Neurosci. Lett.* **548**, 190–195
- Chivet, M., Javalet, C., Hemming, F., Pernet-Gallay, K., Laulagnier, K., Fraboulet, S., and Sadoul, R. (2013) Exosomes as a novel way of interneuronal communication. *Biochem. Soc. Trans.* **41**, 241–244
- Danzer, K. M., Kranich, L. R., Ruf, W. P., Cagsal-Getkin, O., Winslow, A. R., Zhu, L., Vanderburg, C. R., and McLean, P. J. (2012) Exosomal cell-to-cell transmission of α -synuclein oligomers. *Mol. Neurodegener.* **7**, 42
- Alvarez-Erviti, L., Seow, Y., Schapira, A. H., Gardiner, C., Sargent, I. L., Wood, M. J., and Cooper, J. M. (2011) Lysosomal dysfunction increases exosome-mediated α -synuclein release and transmission. *Neurobiol. Dis.* **42**, 360–367
- Pan-Montojo, F., Schwarz, M., Winkler, C., Arnhold, M., O'Sullivan, G. A.,

- Pal, A., Said, J., Marsico, G., Verbavatz, J. M., Rodrigo-Angulo, M., Gille, G., Funk, R. H., and Reichmann, H. (2012) Environmental toxins trigger PD-like progression via increased α -synuclein release from enteric neurons in mice. *Sci. Rep.* **2**, 898
35. Buell, A. K., Galvagnion, C., Gaspar, R., Sparr, E., Vendruscolo, M., Knowles, T. P., Linse, S., and Dobson, C. M. (2014) Solution conditions determine the relative importance of nucleation and growth processes in α -synuclein aggregation. *Proc. Natl. Acad. Sci. U.S.A.* **111**, 7671–7676
36. Grey, M., Linse, S., Nilsson, H., Brundin, P., Sparr, E. (2011) Membrane interaction of α -synuclein in different aggregation states. *J. Parkinsons Dis.* **1**, 359–371
37. Hansen, C., Angot, E., Bergström, A. L., Steiner, J. A., Pieri, L., Paul, G., Outeiro, T. F., Melki, R., Kallunki, P., Fog, K., Li, J. Y., and Brundin, P. (2011) α -Synuclein propagates from mouse brain to grafted dopaminergic neurons and seeds aggregation in cultured human cells. *J. Clin. Invest.* **121**, 715–725
38. Théry, C., Amigorena, S., Raposo, G., and Clayton, A. (2006) Isolation and characterization of exosomes from cell culture supernatants and biological fluids. *Curr. Protoc. Cell Biol.* 2006 Chapter 3, Unit 3.22
39. Lee, B. R., and Kamitani, T. (2011) Improved immunodetection of endogenous α -synuclein. *PLoS ONE* **6**, e23939
40. Bligh, E. G., and Dyer, W. J. (1959) A rapid method of total lipid extraction and purification. *Can. J. Biochem. Physiol.* **37**, 911–917
41. Ejlerskov, P., Rasmussen, L., Nielsen, T. T., Bergström, A. L., Tohyama, Y., Jensen, P. H., and Vilhardt, F. (2013) Tubulin polymerization-promoting protein (TPPP/p25 α) promotes unconventional secretion of α -synuclein through exophagy by impairing autophagosome-lysosome fusion. *J. Biol. Chem.* **288**, 17313–17335
42. Théry, C. (2011) Exosomes: secreted vesicles and intercellular communications. *Fl000 Biol. Rep.* **3**, 15
43. Jaspard, F., Nadi, M., and Rouane, A. (2003) Dielectric properties of blood: an investigation of haematocrit dependence. *Physiol. Meas.* **24**, 137–147
44. Seelert, H., Poetsch, A., Dencher, N. A., Engel, A., Stahlberg, H., and Müller, D. J. (2000) Structural biology. Proton-powered turbine of a plant motor. *Nature* **405**, 418–419
45. Hellstrand, E., Grey, M., Ainalem, M. L., Ankner, J., Forsyth, V. T., Fragneto, G., Haertlein, M., Dauvergne, M. T., Nilsson, H., Brundin, P., Linse, S., Nylander, T., and Sparr, E. (2013) Adsorption of α -synuclein to supported lipid bilayers: positioning and role of electrostatics. *ACS Chem. Neurosci.* **4**, 1339–1351
46. Bartels, T., Choi, J. G., and Selkoe, D. J. (2011) α -Synuclein occurs physiologically as a helically folded tetramer that resists aggregation. *Nature* **477**, 107–110
47. Fauvet, B., Mbefo, M. K., Fares, M. B., Desobry, C., Michael, S., Ardah, M. T., Tsika, E., Coune, P., Prudent, M., Lion, N., Eliezer, D., Moore, D. J., Schneider, B., Aebischer, P., El-Agnaf, O. M., Masliah, E., and Lashuel, H. A. (2012) α -Synuclein in central nervous system and from erythrocytes, mammalian cells, and *Escherichia coli* exists predominantly as disordered monomer. *J. Biol. Chem.* **287**, 15345–15364
48. Giehm, L., and Otzen, D. E. (2010) Strategies to increase the reproducibility of protein fibrillization in plate reader assays. *Anal. Biochem.* **400**, 270–281
49. Rabe, M., Soragni, A., Reynolds, N. P., Verdes, D., Liverani, E., Riek, R., and Seeger, S. (2013) On-surface aggregation of α -synuclein at nanomolar concentrations results in two distinct growth mechanisms. *ACS Chem. Neurosci.* **4**, 408–417
50. Biancalana, M., and Koide, S. (2010) Molecular mechanism of thioflavin-T binding to amyloid fibrils. *Biochim. Biophys. Acta* **1804**, 1405–1412
51. Hellstrand, E., Boland, B., Walsh, D. M., and Linse, S. (2010) Amyloid β -protein aggregation produces highly reproducible kinetic data and occurs by a two-phase process. *ACS Chem. Neurosci.* **1**, 13–18
52. Cohen, S. I., Linse, S., Luheshi, L. M., Hellstrand, E., White, D. A., Rajah, L., Otzen, D. E., Vendruscolo, M., Dobson, C. M., and Knowles, T. P. (2013) Proliferation of amyloid- β 42 aggregates occurs through a secondary nucleation mechanism. *Proc. Natl. Acad. Sci. U.S.A.* **110**, 9758–9763
53. Olofsson, G., and Sparr, E. (2013) Ionization constants pK_a of cardiolipin. *PLoS ONE* **8**, e73040
54. Rouser, G., Fkeischer, S., and Yamamoto, A. (1970) Two-dimensional thin layer chromatographic separation of polar lipids and determination of phospholipids by phosphorus analysis of spots. *Lipids* **5**, 494–496
55. Hellstrand, E., Nowacka, A., Topgaard, D., Linse, S., and Sparr, E. (2013) Membrane lipid co-aggregation with α -synuclein fibrils. *PLoS ONE* **8**, e77235
56. Kucerka, N., Tristram-Nagle, S., and Nagle, J. F. (2005) Structure of fully hydrated fluid phase lipid bilayers with monounsaturated chains. *J. Membr. Biol.* **208**, 193–202
57. Martinez, Z., Zhu, M., Han, S., and Fink, A. L. (2007) GM1 specifically interacts with α -synuclein and inhibits fibrillation. *Biochemistry* **46**, 1868–1877
58. Uversky, V. N., Li, J., and Fink, A. L. (2001) Evidence for a partially folded intermediate in α -synuclein fibril formation. *J. Biol. Chem.* **276**, 10737–10744
59. Trexler, A. J., and Rhoades, E. (2009) α -Synuclein binds large unilamellar vesicles as an extended helix. *Biochemistry* **48**, 2304–2306
60. Cabaleiro-Lago, C., Quinlan-Pluck, F., Lynch, I., Dawson, K. A., and Linse, S. (2010) Dual effect of amino modified polystyrene nanoparticles on amyloid β protein fibrillation. *ACS Chem. Neurosci.* **1**, 279–287
61. Devi, L., Raghavendran, V., Prabhu, B. M., Avadhani, N. G., and Anandatheerthavada, H. K. (2008) Mitochondrial import and accumulation of α -synuclein impair complex I in human dopaminergic neuronal cultures and Parkinson disease brain. *J. Biol. Chem.* **283**, 9089–9100
62. Scott, C. C., and Gruenberg, J. (2011) Ion flux and the function of endosomes and lysosomes: pH is just the start. *BioEssays* **33**, 103–110
63. Cole, N. B., Dieuliis, D., Leo, P., Mitchell, D. C., and Nussbaum, R. L. (2008) Mitochondrial translocation of α -synuclein is promoted by intracellular acidification. *Exp. Cell Res.* **314**, 2076–2089
64. Svensson, K. J., Christianson, H. C., Wittrup, A., Bourseau-Guilmain, E., Lindqvist, E., Svensson, L. M., Mörgelin, M., and Belting, M. (2013) Exosome uptake depends on ERK1/2-heat shock protein 27 signaling and lipid raft-mediated endocytosis negatively regulated by caveolin-1. *J. Biol. Chem.* **288**, 17713–17724
65. Middleton, E. R., and Rhoades, E. (2010) Effects of curvature and composition on α -synuclein binding to lipid vesicles. *Biophys. J.* **99**, 2279–2288
66. Nakamura, K., Nemani, V. M., Azarbal, F., Skibinski, G., Levy, J. M., Egami, K., Munishkina, L., Zhang, J., Gardner, B., Wakabayashi, J., Sesaki, H., Cheng, Y., Finkbeiner, S., Nussbaum, R. L., Masliah, E., and Edwards, R. H. (2011) Direct membrane association drives mitochondrial fission by the Parkinson disease-associated protein α -synuclein. *J. Biol. Chem.* **286**, 20710–20726
67. Stöckl, M., Fischer, P., Wanker, E., and Herrmann, A. (2008) α -Synuclein selectively binds to anionic phospholipids embedded in liquid-disordered domains. *J. Mol. Biol.* **375**, 1394–1404
68. Futerman, A. H., and Hannun, Y. A. (2004) The complex life of simple sphingolipids. *EMBO Rep.* **5**, 777–782
69. Hoshino, T., Mahmood, M. I., Mori, K., and Matsuzaki, K. (2013) Binding and aggregation mechanism of amyloid β -peptides onto the GM1 ganglioside-containing lipid membrane. *J. Phys. Chem. B* **117**, 8085–8094
70. Sani, M. A., Gehman, J. D., and Separovic, F. (2011) Lipid matrix plays a role in A β fibril kinetics and morphology. *FEBS Lett.* **585**, 749–754
71. Okada, T., Ikeda, K., Wakabayashi, M., Ogawa, M., and Matsuzaki, K. (2008) Formation of toxic A β (1–40) fibrils on GM1 ganglioside-containing membranes mimicking lipid rafts: polymorphisms in A β (1–40) fibrils. *J. Mol. Biol.* **382**, 1066–1074
72. Linse, S., Cabaleiro-Lago, C., Xue, W. F., Lynch, I., Lindman, S., Thulin, E., Radford, S. E., and Dawson, K. A. (2007) Nucleation of protein fibrillation by nanoparticles. *Proc. Natl. Acad. Sci. U.S.A.* **104**, 8691–8696
73. Pfefferkorn, C. M., Heinrich, F., Sodt, A. J., Maltsev, A. S., Pastor, R. W., and Lee, J. C. (2012) Depth of α -synuclein in a bilayer determined by fluorescence, neutron reflectometry, and computation. *Biophys. J.* **102**, 613–621
74. Arosio, P., Cukalevski, R., Frohm, B., Knowles, T. P., and Linse, S. (2014) Quantification of the concentration of A β 42 propagons during the lag phase by an amyloid chain reaction assay. *J. Am. Chem. Soc.* **136**, 219–225
75. Meisl, G., Yang, X., Hellstrand, E., Frohm, B., Kirkegaard, J. B., Cohen, S. I., Dobson, C. M., Linse, S., and Knowles, T. P. (2014) Differences in nucleation behaviour underlie the contrasting aggregation pathways of the

Exosomes Catalyze α -Synuclein Aggregation

- A β 40 and A β 42 peptide. *Proc. Natl. Sci. Acad. U.S.A.* **111**, 9384–9389
76. Yanagisawa, K., Odaka, A., Suzuki, N., and Ihara, Y. (1995) GM1 ganglioside-bound amyloid β -protein (A β): a possible form of preamyloid in Alzheimer's disease. *Nat. Med.* **1**, 1062–1066
77. Ariga, T., McDonald, M. P., and Yu, R. K. (2008) Role of ganglioside metabolism in the pathogenesis of Alzheimer's disease—a review. *J. Lipid Res.* **49**, 1157–1175
78. Hong, S., Ostaszewski, B. L., Yang, T., O'Malley, T. T., Jin, M., Yanagisawa, K., Li, S., Bartels, T., and Selkoe, D. J. (2014) Soluble A β oligomers are rapidly sequestered from brain ISF *in vivo* and bind GM1 ganglioside on cellular membranes. *Neuron* **82**, 308–319
79. Kakio, A., Nishimoto, S. I., Yanagisawa, K., Kozutsumi, Y., and Matsuzaki, K. (2001) Cholesterol-dependent formation of GM1 ganglioside-bound amyloid β -protein, an endogenous seed for Alzheimer amyloid. *J. Biol. Chem.* **276**, 24985–24990
80. Matsuzaki, K., Kato, K., and Yanagisawa, K. (2010) A β polymerization through interaction with membrane gangliosides. *Biochim. Biophys. Acta* **1801**, 868–877
81. Vingtdeux, V., Sergeant, N., and Buée, L. (2012) Potential contribution of exosomes to the prion-like propagation of lesions in Alzheimer's disease. *Front. Physiol.* **3**, 229
82. Keilani, S., Lun, Y., Stevens, A. C., Williams, H. N., Sjoberg, E. R., Khanna, R., Valenzano, K. J., Checler, F., Buxbaum, J. D., Yanagisawa, K., Lockhart, D. J., Wustman, B. A., and Gandy, S. (2012) Lysosomal dysfunction in a mouse model of Sandhoff disease leads to accumulation of ganglioside-bound amyloid- β peptide. *J. Neurosci.* **32**, 5223–5236
83. Dehay, B., Martinez-Vicente, M., Ramirez, A., Perier, C., Klein, C., Vila, M., and Bezdard, E. (2012) Lysosomal dysfunction in Parkinson disease: ATP13A2 gets into the groove. *Autophagy* **8**, 1389–1391
84. Dehay, B., Martinez-Vicente, M., Caldwell, G. A., Caldwell, K. A., Yue, Z., Cookson, M. R., Klein, C., Vila, M., and Bezdard, E. (2013) Lysosomal impairment in Parkinson's disease. *Mov. Disord.* **28**, 725–732
85. Michel, C. H., Kumar, S., Pinotsi, D., Tunnacliffe, A., St George-Hyslop, P., Mandelkow, E., Mandelkow, E. M., Kaminski, C. F., and Kaminski Schierle, G. S. (2014) Extracellular monomeric Tau is sufficient to initiate the spread of Tau pathology. *J. Biol. Chem.* **289**, 956–967